

# Vacuolar sequential exocytosis of large dense-core vesicles in adrenal medulla

Takuya Kishimoto<sup>1,2,6</sup>, Ryoichi Kimura<sup>2,3,6</sup>,  
Ting-Ting Liu<sup>1,4</sup>, Tomomi Nemoto<sup>2,5</sup>,  
Noriko Takahashi<sup>1,2,5</sup> and Haruo Kasai<sup>1,2,\*</sup>

<sup>1</sup>Division of Biophysics, Center for Disease Biology and Integrative Medicine, Faculty of Medicine, University of Tokyo, Hongo, Tokyo, Japan, <sup>2</sup>Department of Cell Physiology, National Institute for Physiological Sciences, and Graduate University of Advanced Studies (SOKENDAI), Myodaiji, Okazaki, Japan, <sup>3</sup>Department of Physiology, Hirosaki University School of Medicine, Hirosaki, Japan, <sup>4</sup>Genome Research Center, National Yang-Ming University, Taipei, Taiwan and <sup>5</sup>Precursory Research for Embryonic Science and Technology (PRESTO), Japan Science and Technology Agency, Kawaguchi, Saitama, Japan

**Individual exocytic events in intact adrenal medulla were visualized by two-photon extracellular polar-tracer imaging. Exocytosis of chromaffin vesicles often occurred in a sequential manner, involving first vesicles located at the cell periphery and then those present deeper within the cytoplasm. Sequential exocytosis occurred preferentially at regions of the plasma membrane facing the intercellular space. The compound vesicles swelled to more than five times their original volume and formed vacuolar exocytic lumens as a result of expansion of intravesicular gels and their confinement within the lumen by the fusion pore and the narrow intercellular space. Such luminal swelling greatly promoted sequential exocytosis. The SNARE protein SNAP25 rapidly migrated from the plasma membrane to the membrane of fused vesicles. These data indicate that vesicles present deeper within the cytoplasm can be fusion ready like those at the cell periphery, and that swelling of exocytic lumens promotes assembly of the fusion machinery. We suggest the existence of two molecular configurations for fusion-ready states in Ca<sup>2+</sup>-dependent exocytosis.**

*The EMBO Journal* (2006) 25, 673–682. doi:10.1038/sj.emboj.7600983; Published online 9 February 2006

**Subject Categories:** membranes & transport; neuroscience

**Keywords:** calcium; chromaffin cell; exocytosis; fusion

## Introduction

It has been proposed that exocytosis of secretory vesicles occurs at the cell periphery in neurons and other secretory cells, and that secretory vesicles must be transported to the cell periphery in order to acquire fusion competence before cell stimulation (Martin, 1997; Neher, 1998; Kasai, 1999). Indeed, most instances of exocytosis of insulin vesicles have

been detected at the cell periphery of  $\beta$  cells in islets of Langerhans (Takahashi *et al.*, 2002). Recent studies have revealed a phenomenon referred to as sequential compound exocytosis, however, in which omega ( $\Omega$ )-shaped profiles of vesicles persist at the site of exocytosis after fusion and become targets for exocytosis of vesicles in the deeper layers of the cytoplasm in a variety of secretory cell types, including exocrine acinar cells (Nemoto *et al.*, 2001; Pickett *et al.*, 2005), mast cells (Alvarez de Toledo and Fernandez, 1990), lactotrophs (Angleson *et al.*, 1999), pancreatic  $\beta$  cells (Takahashi *et al.*, 2004), and PC12 cells (Kishimoto *et al.*, 2005). It has remained unclear how the fusion readiness of vesicles deep within the cytoplasm differs from that of those at the cell periphery.

To investigate the spatial organization of exocytosis, we have developed an experimental approach based on two-photon excitation imaging with extracellular polar tracers (Nemoto *et al.*, 2001; Takahashi *et al.*, 2002), systematically described recently as TEP (two-photon extracellular polar-tracer) imaging (Kasai *et al.*, 2005). TEP imaging allows investigation of exocytosis occurring deep within tissues as well as quantitation of the spatial organization of exocytosis and the fates of fused vesicles, feats that have not been possible with classical approaches such as measurement of membrane capacitance, amperometry, and evanescent field microscopy.

We have now applied TEP imaging to semi-intact preparations of adrenal medulla and thereby discovered a novel phenomenon, designated ‘vacuolar sequential exocytosis,’ in which exocytic vesicles swell to more than five times their original volume during sequential exocytosis and form a round exocytic lumen. Formation of vacuoles after exocytosis in chromaffin cells was described in early electron microscopic investigations (Benedeczky and Somogyi, 1975; Baker and Knight, 1981; Furuya *et al.*, 1989), but the underlying mechanism has not previously been elucidated. We have found that vacuolar sequential exocytosis results from the swelling of gels that are present within fused vesicles and which remain confined to the vesicles by the fusion pore and extracellular matrix. The identification of vacuolar sequential exocytosis also allowed us to examine the fusion readiness of vesicles present deep within the cytoplasm. We found that the fusion readiness of deep vesicles located within 2  $\mu$ m from the plasma membrane was similar to that of peripheral vesicles, and that lateral diffusion of the SNARE protein SNAP25 appeared to be necessary for sequential exocytosis. Our data suggest the existence of two fusion-ready molecular configurations in Ca<sup>2+</sup>-dependent exocytosis of vesicles in neurons and secretory cells.

## Results

### Vacuolar sequential exocytosis

We studied small fragments of adrenal medulla, comprising clusters of ~3–10 chromaffin cells, that had been cultured for

\*Corresponding author. Division of Biophysics, Center for Disease Biology and Integrative Medicine, Faculty of Medicine, University of Tokyo, Hongo, Tokyo 113-0033, Japan.

Tel.: +81 3 5841 1439; Fax: +81 3 5841 1442;

E-mail: hkasai@m.u-tokyo.ac.jp

<sup>6</sup>These authors contributed equally to this work

Received: 31 October 2005; accepted: 11 January 2006; published online: 9 February 2006

1–5 days. The cell clusters were investigated with TEP imaging, for which they were immersed in a solution containing a fluid-phase tracer, sulforhodamine B (SRB) (Figure 1A). This preparation preserved the original multicellular organization of the tissue, with each chromaffin cell being surrounded by narrow (20–40 nm) intercellular spaces (Figure 1A) (Benedeczky and Somogyi, 1975). Stimulation of the cell clusters with a high concentration (70 mM) of  $K^+$  resulted in the rapid appearance of many fluorescent spots adjacent to such intercellular spaces (Figure 1A and Supplementary Movie 1). The abrupt onset of fluorescence indicated that these spots represented exocytosis (Figure 1B and C). Moreover, secretory vesicles collapsed almost completely into the plasma membrane in 16% of exocytic events ( $n = 130$ ), with vesicle flattening requiring only a fraction of a

second (Figure 1B and C). Fused vesicles remained poised at the site of exocytosis in 12% of vesicles (Figure 1D and E), likely reflecting the kiss-and-stay exo-endocytosis (see Figure 8F) (Sudhof, 2004). Most vesicles (72%), however, appeared to swell after fusion (Figure 1F), and fluorescence was gradually increased after exocytosis (Figure 1G). In 63% of fused vesicles, such gradual swelling was accompanied by abrupt appearance of fluorescent spot (Figure 1H, arrowhead and arrow), indicating that vesicles located deeper within the cytoplasm underwent exocytosis toward the swelling vesicles (Figure 1I). Secondary exocytic vesicles merged with the luminal plasma membrane in <1 s (Figure 1H and J, arrow).

The full-width at half-maximal (FWHM) diameters of the primary ( $0.50 \pm 0.08 \mu\text{m}$ , mean  $\pm$  s.e.m.,  $n = 128$ ) and secondary exocytic vesicles were similar ( $0.50 \pm 0.09 \mu\text{m}$ ,  $n = 58$ )

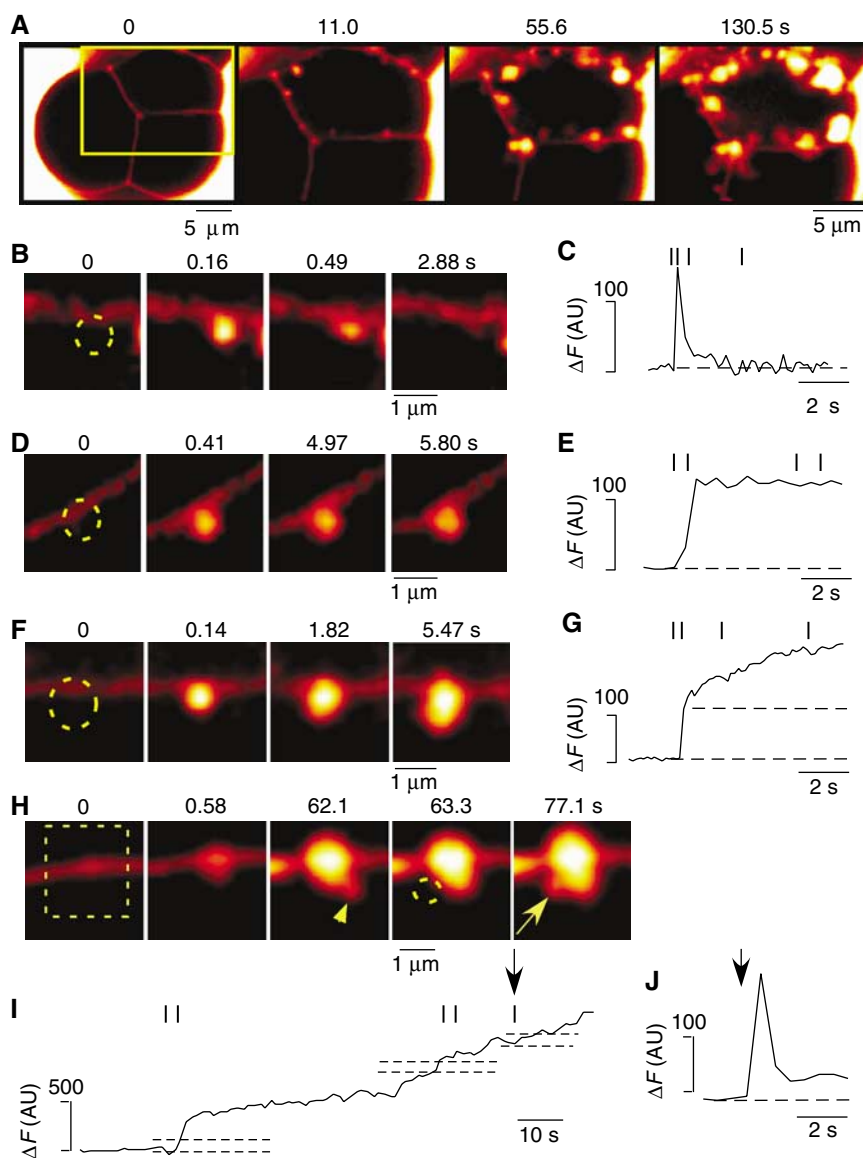


**Figure 1** Exocytic events visualized by TEP imaging of adrenal medullary cell clusters immersed in a solution containing SRB. (A) Vacuolar sequential exocytosis induced by high- $K^+$  stimulation in bovine adrenal medulla (see Supplementary Movie 1). Numbers indicate time after the onset of stimulation. The region outlined by the yellow box in the left panel is shown in close-up in the other panels. (B, D, F, H) A full-fusion exocytic event at the primary plasma membrane (B), kiss-and-stay exo-endocytosis (D), swelling of a vesicle after exocytosis at the primary plasma membrane (F), and formation of an exocytic lumen as a result of sequential exocytosis and swelling (H). The arrow and arrowhead in (H) indicate fusion of deep vesicles with the exocytic lumen. (C, E, G, I, J) Increases in SRB fluorescence intensity ( $\Delta F$ ), expressed in arbitrary units (AU), corresponding to the regions outlined by the dashed circles in (B), (D), and (F) and the dashed square and circle in (H), respectively.

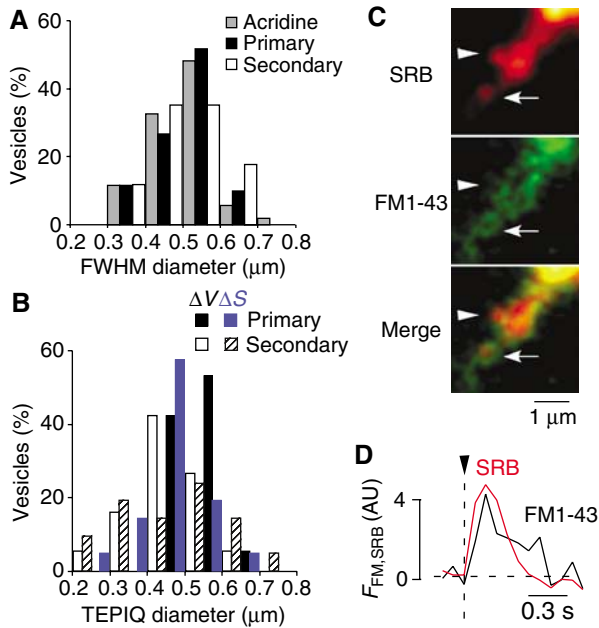


**Figure 2** Diameters of exocytic vesicles estimated with SRB and FM1-43. **(A)** Histograms of FWHM diameters, for fluorescence spots corresponding to vesicles stained with acridine orange or to primary or secondary exocytic events stained with SRB and induced by stimulation with high- $K^+$  solution. **(B)** Histograms of diameters of exocytic vesicles estimated by TEPIQ analyses of  $\Delta V$  and  $\Delta S$ . The fluorescence intensities were converted into volume and surface areas as described (Kasai *et al*, 2005) to obtain diameters of primary and secondary exocytic vesicles. **(C)** Simultaneous staining of exocytosis with SRB and FM1-43. The arrow and arrowhead show primary and secondary exocytic vesicles, respectively. **(D)** Time courses of staining of the secondary exocytic vesicle with SRB and FM1-43.

and were consistent with those of chromaffin vesicles stained with acridine orange ( $0.51 \pm 0.08 \mu\text{m}$ ,  $n = 52$ ) (Figure 2A). The mean diameters of primary and secondary vesicles were similarly estimated as  $0.51 \pm 0.4 \mu\text{m}$  ( $n = 19$ ) and  $0.47 \pm 0.09 \mu\text{m}$  ( $n = 18$ ), respectively (Figure 2B, black bars), also with TEPIQ (TEP imaging-based quantification) analysis of  $\Delta V$  (Kasai *et al*, 2005), which measures the volume of the vesicle by fluorescent intensity of SRB, and can estimate the vesicle diameter independently of spatial resolution of the microscope. The exocytosis was also rapidly labeled with FM1-43 (Figure 2C and D), which estimated the diameter of primary and secondary vesicles as  $0.46 \pm 0.07 \mu\text{m}$  ( $n = 21$ ) and  $0.48 \pm 0.14 \mu\text{m}$  ( $n = 18$ ), respectively, with TEPIQ analysis of  $\Delta S$  (Figure 2B) (Kasai *et al*, 2005). Diameters of vesicles were similarly estimated with an electron microscope (Furuya *et al*, 1989; Fox, 1996). These results indicate that the fluorescent spots represent exocytosis of single chromaffin vesicles. Vesicles therefore did not fuse with each other before exocytosis (a process known as multigranular compound exocytosis) (Takahashi *et al*, 2004), consistent with the smooth increase in membrane capacitance of chromaffin cells, previously observed during stimulation (Chow *et al*, 1996; Ninomiya *et al*, 1997; Haller *et al*, 1998).

Sequential exocytosis resulted in the formation of a round exocytic lumen (Figure 1A), which often spanned a distance of 2–3  $\mu\text{m}$  from the plasma membrane (Figure 3A–C). We found that this ‘vacuolar sequential exocytosis’ occurred infrequently at the region of the plasma membrane directly

facing the external medium (Figures 1A, 3A, and C, blue line) with a frequency of 0.61 and 0.03 events  $\text{min}^{-1} \mu\text{m}^2$  toward the intercellular space and external medium, respectively. This observation likely explains why the phenomenon has not been detected in studies performed with isolated chromaffin cells, although similar vacuolar structures have been described in electron microscopic investigations of these cells (Benedeczky and Somogyi, 1975; Baker and Knight, 1981; Furuya *et al*, 1989; Fox, 1996).

Formation of exocytic lumens was reversible and repeatable. The lumens (Supplementary Figure 1A) thus gradually shrank after cessation of stimulation (Supplementary Figure 1B), possibly as a result of classical endocytic mechanisms. Moreover, formation of exocytic lumens could be induced repeatedly during a second round of stimulation (Supplementary Figure 1C). These data support the notion that vacuolar sequential exocytosis is a physiological response of chromaffin cells to a high level of stimulation. Sequential exocytosis was far infrequent during weaker stimulation (see Figure 5A, within 10 s after stimulation).

Vacuolar sequential exocytosis was also detected in cells stimulated by homogeneous and rapid increases in the cytosolic  $\text{Ca}^{2+}$  concentration ( $[\text{Ca}^{2+}]_i$ ) induced by uncaging of a caged- $\text{Ca}^{2+}$  compound, *o*-nitrophenyl EGTA (NPE; Figure 3E–G and Supplementary Movie 2). Again, such exocytosis was infrequent in the portion of the plasma membrane directly facing the external medium (Figure 3E and G, blue line). The major features of vacuolar sequential exocytosis thus did not depend on the  $\text{Ca}^{2+}$  gradients formed by the opening of voltage-gated  $\text{Ca}^{2+}$  channels. The increase in  $[\text{Ca}^{2+}]_i$  induced by uncaging of NPE was estimated as 20–40  $\mu\text{M}$  with the use of the  $\text{Ca}^{2+}$  indicator fura-2FF, and it decayed with a time constant of 6–15 s (Figure 3H). The exocytic lumens extended to a distance of  $1.4 \pm 0.1 \mu\text{m}$  (mean  $\pm$  s.e.m.,  $n = 8$ ) from the primary plasma membrane within 10 s (Figure 3F and G). In contrast, the exocytic lumens grew more slowly and deeper ( $1.9 \pm 0.1 \mu\text{m}$  within 45 s,  $n = 14$ ) in cells stimulated with high- $K^+$  solution (Figure 3B and C), which resulted in a smaller but more persistent increase in  $[\text{Ca}^{2+}]_i$  (Figure 3D).

#### Rate of exocytosis per membrane area

To obtain the rate of exocytosis per membrane area, we first estimated the areas of the primary and luminal plasma membrane. We estimated the primary plasma membrane area as  $S_p(t) = 2\pi R(t)T$ , where  $R(t)$  represents the radius of the cell and  $T$  the  $z$ -axis depth of images in which exocytosis was detected and was 2  $\mu\text{m}$  in our setup (see Materials and methods). The primary plasma membrane area thus obtained from the radius of the cell remained unaltered during vacuolar sequential exocytosis (Figure 4A and B). We defined the luminal membrane as the plasma membrane other than the primary plasma membrane. The lack of an increase in the primary plasma membrane area indicated that the luminal membrane area accounts for all the increases in the membrane area caused by both secondary and primary exocytosis.

The luminal plasma membrane area ( $S_L(t)$ ) was estimated by fitting each lumen with a circle of radius  $R_i(t)$ , as a first approximation, and then calculating the sum as  $S_L(t) = \sum_i 2\pi R_i(t)T$  (Figure 3A and B). We found that  $S_L(t)$  was proportional to the cumulative number of exocytic events at both the primary ( $N_p(t)$ ) and luminal ( $N_L(t)$ ) plasma

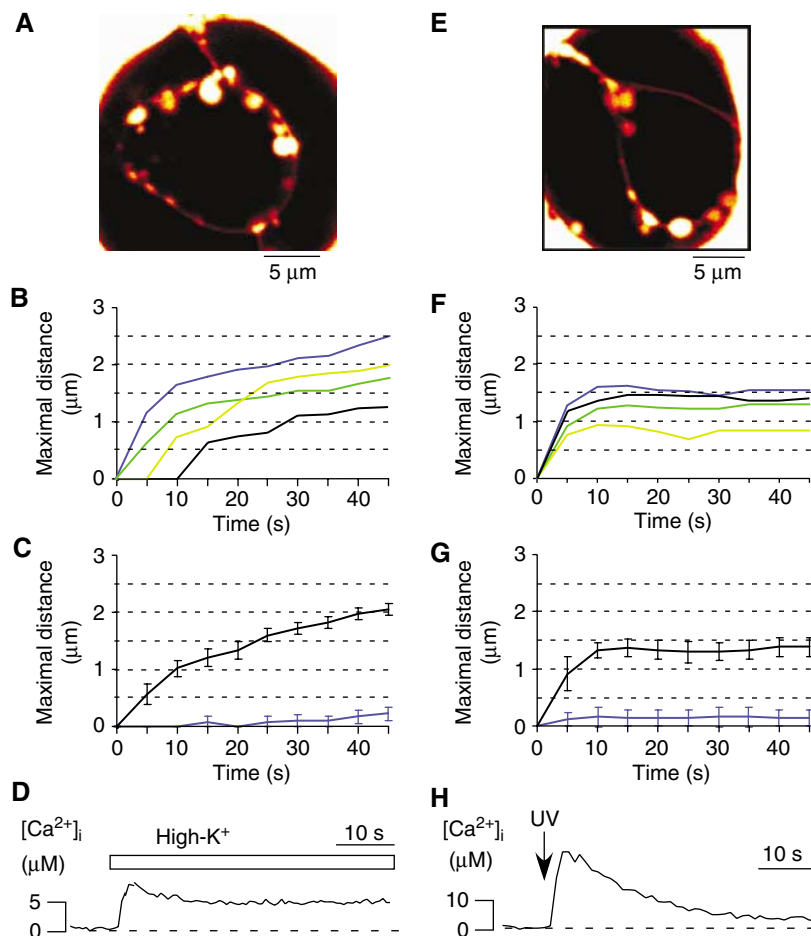


**Figure 3** Progression of vacuolar sequential exocytosis. **(A)** Vacuolar sequential exocytosis induced by high- $K^+$  solution. The image was captured 130 s after the onset of stimulation. **(B, C, F, G)** Growth of exocytic lumens represented by the maximal distance of the lumen from the primary plasma membrane during stimulation with high- $K^+$  solution (**B, C**) or by uncaging of NPE (**F, G**). Data from individual cells are shown in different colors in (**B**) and (**F**), and means  $\pm$  s.e.m. of values from eight or 14 cells are shown in (**C**) and (**G**), respectively. Black and blue lines in (**C**) and (**G**) correspond to exocytic lumens formed at regions of the plasma membrane facing the intercellular space and the extracellular medium, respectively. **(E)** Vacuolar sequential exocytosis induced by uncaging of NPE (see Supplementary Movie 2). The image was captured 64 s after uncaging of NPE. **(D, H)** Time courses of  $[Ca^{2+}]_i$  measured with fura-2FF in individual cells stimulated with high- $K^+$  solution or by ultraviolet (UV) radiation-induced uncaging of NPE, respectively.

membrane (Figure 4C) with a correlation coefficient of 0.97 ( $n = 126$ ). Moreover, the regression coefficients of such plots were used to estimate the fractional detection of exocytosis ( $\alpha$ ) from  $\alpha = 4\pi d^2(N_P + N_L)/S_L$ , assuming a vesicle diameter ( $d$ ) of  $0.5 \mu\text{m}$ . The fractional detection was larger in experiments with higher rates of image acquisition (Figure 4D). The fact that  $\alpha$  was only 0.5 even at a sampling rate of 2 Hz suggests that the mean lifetime of  $\Omega$  profiles was  $\sim 0.25$  s ( $0.5/2$ ). Indeed, the lifetime was estimated as  $0.25 \pm 0.1$  s ( $n = 5$ ) at a rate of image acquisition of 9 Hz (data not shown). These results are consistent with the notion that exocytic lumens form as a direct consequence of sequential exocytosis, and they suggest that we properly estimated the luminal membrane area. In most imaging experiments, we used relatively low sampling rates (0.5–2 Hz) to obtain high-quality images from broad cellular areas.

The rate per cell ( $N'(t)$ ,  $\text{min}^{-1} \text{cell}^{-1}$ ) was greater for primary exocytosis than for secondary exocytosis at the beginning ( $< 10$  s) of stimulation either with high- $K^+$  solution (Figure 5A) or by uncaging of NPE (Figure 5B). Most (70%) exocytic events, however, were attributable to secondary exocytosis after longer periods of stimulation ( $> 20$  s)

with high- $K^+$  solution (Figure 5A), for which the formation of exocytic lumens was more extensive than that elicited by uncaging of NPE. The prevalence of secondary exocytosis at the luminal membrane suggested that deep vesicles were in fact mobilized for exocytosis.

The rate of exocytosis per unit membrane area ( $\text{min}^{-1} \mu\text{m}^{-2}$ ) was obtained by dividing  $N'(t)$  with  $S(t)$  for primary and luminal plasma membrane (Figure 5C and D). The rate ( $N'(t)/S(t)$ ) of secondary exocytosis was greater than that for primary exocytosis during most of the period of stimulation (Figure 5C and D). The mean rate obtained within 30 s after the onset of stimulation was thus larger for secondary exocytosis ( $\sim 0.62 \text{ events min}^{-1} \mu\text{m}^{-2}$ ) than for primary exocytosis ( $\sim 0.35 \text{ events min}^{-1} \mu\text{m}^{-2}$ ) in cells stimulated with high- $K^+$  solution (Figure 6A) or by uncaging of NPE. These results indicate that vesicles in the deeper layers of the cytoplasm possess a fusion readiness similar to or even greater than that of those at the periphery in stimulated chromaffin cells present within the intact adrenal medulla, given that vesicles are homogeneously distributed in chromaffin cells (Benedeczy and Somogyi, 1975; Plattner *et al*, 1997).

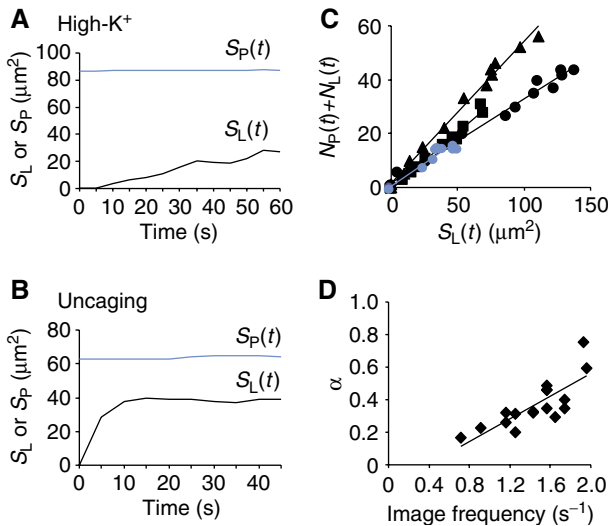


**Figure 4** Areas of the primary and luminal plasma membrane and the total number of exocytic events in individual chromaffin cells. (A, B) Areas of the primary plasma membrane ( $S_P(t)$ ) and of the luminal plasma membrane ( $S_L(t)$ ) in representative cells during stimulation with high- $K^+$  solution (A) or by uncaging of NPE (B) are indicated by blue and black lines, respectively. (C) Correlation between the area of the luminal plasma membrane ( $S_L(t)$ ) and the cumulative number of exocytic events at both the primary and luminal plasma membrane ( $N_P(t) + N_L(t)$ ) in individual cells. Data from four cells are depicted with different symbols; the blue symbols correspond to a cell stimulated by uncaging of NPE. (D) Efficiency of detection of exocytosis ( $\alpha$ ) versus the rate of image acquisition. The efficiency values were obtained from the slope of plots similar to those shown in (C) and the mean vesicle diameter ( $d = 0.5 \mu\text{m}$ ) according to the relation  $\alpha = 4\pi d^2(N_P + N_L)/S_L$ .

### Vesicle swelling

Our results suggested that the contents of vesicles swell markedly during vacuolar sequential exocytosis. We quantified such swelling in individual cells from the ratio ( $A(t)/B(t)$ ) between the total volume of lumens,  $A(t) = \sum_i \pi R_i(t)^2 T$ , and the predicted original volume of the vesicles that underwent exocytosis to form the lumens,  $B(t) = N_L(t)(4/3\alpha)\pi d^3$ . For this analysis, we selected lumens with a largely circular profile and determined the fractional detection of exocytosis ( $\alpha$ ) for the corresponding cells. The analysis indicated that swelling occurred rapidly, with a time constant of 10 s, and that the final luminal volume was about five times the original volume of the vesicles in cells stimulated with high- $K^+$  solution or by uncaging of NPE (Figure 6B). The swelling in cells stimulated by large increases in  $[\text{Ca}^{2+}]_i$  induced by uncaging of NPE was greatly inhibited when the colloid osmotic pressure of the extracellular solution was increased with Ficoll (14%, 400 kDa) (Figure 6B), indicating that it was attributable to expansion of hydrogels in the vesicle matrix (Tanaka *et al*, 1982; Zimmerberg *et al*, 1987; Nanavati and Fernandez, 1993). In fact, the pressure in lumens appeared to be more positive than that in the cytosol, as the swelling was markedly reduced, but still present, when exocytosis was induced with a hypotonic high- $K^+$  solution (230 versus 310 mOsm in the normal external solution), which caused marked swelling of the cytosol (data not shown).

We found that vesicle swelling promoted secondary exocytosis at the luminal membrane. In the presence of Ficoll, sequential exocytosis occurred with little vesicle swelling

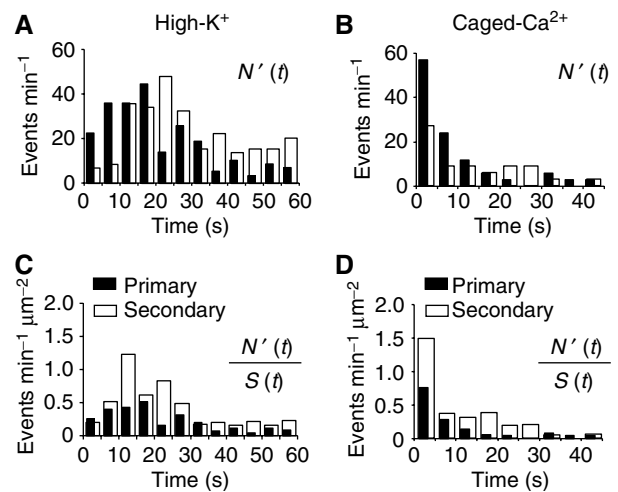


**Figure 5** Rates of exocytosis per cell ( $N'(t)$ ) and per unit membrane area ( $N'(t)/S(t)$ ) for primary and secondary exocytosis. (A, B) Rates of exocytosis, expressed as the number of exocytic events per minute, for primary exocytosis at the primary plasma membrane ( $N'_P(t)$ , closed bars) and for secondary exocytosis at the luminal plasma membrane ( $N'_L(t)$ , open bars) during high- $K^+$  stimulation in eight cells (A) and after uncaging of NPE in six cells (B). The total number of events was divided by the number of cells examined. (C, D) Rates of exocytosis, expressed as the number of exocytic events per minute per unit membrane area, at the primary plasma membrane ( $N'_P(t)/S_P(t)$ , closed bars) and at the luminal plasma membrane ( $N'_L(t)/S_L(t)$ , open bars) during high- $K^+$  stimulation (C) and after uncaging of NPE (D). The rates were obtained from the total values of  $N'(t)$  and  $S(t)$  in the sets of cells shown in (A) and (B) at intervals of 5 s.

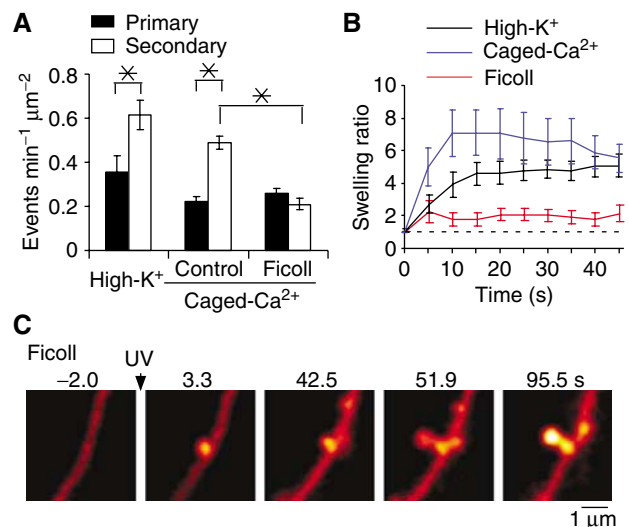


**Figure 6** Dependence of the rates of exocytosis per membrane area on luminal swelling. (A) Rates of exocytosis per unit area of the primary or luminal plasma membrane in cells stimulated either with a high- $K^+$  solution or by uncaging of NPE in the absence or presence of 14% Ficoll. The values of  $N'(t)/S(t)$  were obtained for each cell as in Figure 4 and were averaged for the initial 30 s after the onset of stimulation and for 5–10 cells. Data are means  $\pm$  s.e.m.;  $*P < 0.05$  for the indicated comparisons (Student's *t*-test). (B) Swelling ratios, calculated as described in the text, for cells stimulated with a high- $K^+$  solution (black line,  $n = 14$ ) or by uncaging of NPE in the absence (blue line,  $n = 8$ ) or presence (red line,  $n = 9$ ) of Ficoll. Data are means  $\pm$  s.e.m. (C) Preservation of original  $\Omega$ -shaped profiles in a cell stimulated by uncaging of NPE in the presence of Ficoll.

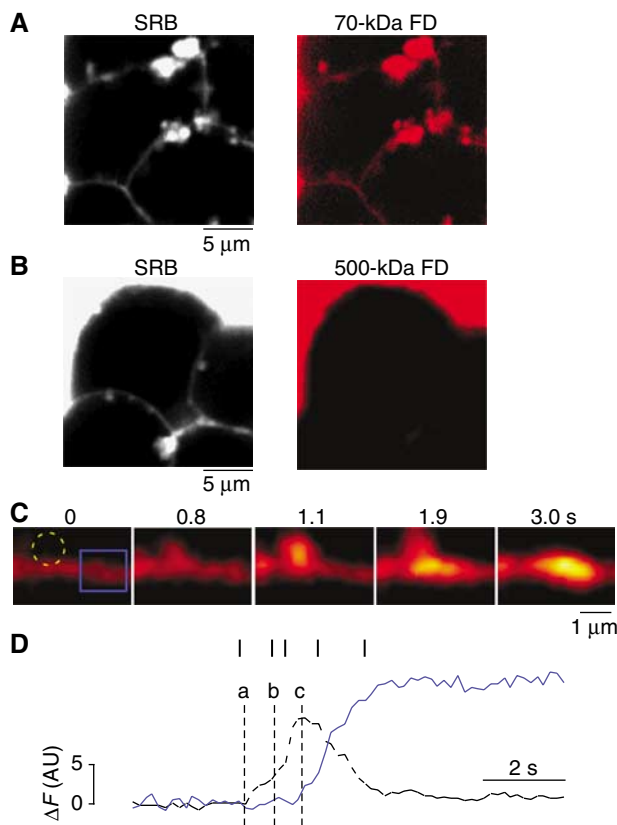


**Figure 7** The intercellular space as a diffusion barrier. (A, B) Adrenal medullary preparations were immersed in a solution containing SRB and either 70-kDa (A) or 500-kDa (B) fluorescein dextran (FD) for 30 min. Images were obtained 13 s after uncaging of NPE, a time when exocytic lumens were detected in the SRB images. (C) A full-fusion event for a single vesicle in which swelling of the vesicle contents was followed by their release and their further swelling in the intercellular space (see Supplementary Movie 3). (D) Time courses of fluorescence for the vesicle (dashed circle in (C), dashed line in (D)) and for the intercellular space (blue square in (C), blue line in (D)) corresponding to the event shown in (C). The onsets of exocytosis, swelling, and full fusion are denoted by vertical lines a, b, and c, respectively.

(Figure 6C) and round exocytic lumens were rarely seen. Ficoll did not reduce the rate of primary exocytosis per unit membrane area (Figure 6A), indicating that it did not affect the fusion reaction itself. It did, however, markedly reduce the rate of secondary exocytosis (Figure 6A), with the result that the deeper vesicles showed a rate of exocytosis similar to or less than that of the peripheral ones.

The mechanism by which the swelling of vesicle hydrogels is triggered during exocytosis remains to be determined. It was not simply mediated by alkalization of the vesicle contents after opening of the fusion pore, given that vacuolar sequential exocytosis was similarly induced in an external solution whose pH was adjusted to 5.0 (data not shown). It was also not simply mediated by exchange of inorganic ions bound to the gels, because vacuolar sequential exocytosis was similarly elicited in an external solution in which most external ions were replaced by sucrose (260 mM sucrose, 10 mM glucose, 10 mM HEPES-Ca(OH)<sub>2</sub> (pH 7.4)) (data not shown). It is possible that the swelling requires the release of intrinsic molecules that are bound to the gels and which prevent gel swelling before exocytosis.

### Role of the extracellular matrix and fusion pore

Swelling of the exocytic lumen would be expected to depend on prevention of diffusion of the hydrogels into the intercellular space. We found that the intercellular space of intact adrenal medullary tissue allowed diffusion of 70-kDa fluorescein dextran, as it did that of SRB (Figure 7A), but not that of 500-kDa fluorescein dextran (Figure 7B). Given that the hydrodynamic diameters of 70- and 500-kDa fluorescein dextran are 12 and 20 nm, respectively, these observations are consistent with the fact that the intercellular space is as narrow as 20–40 nm (Benedeczky and Somogyi, 1975). In addition, high rates of acquisition of images of full-fusion exocytosis revealed that 36% of such events ( $n=28$ ) were accompanied by swelling of the vesicle contents after their release into the intercellular space (Figure 7C and D and Supplementary Movie 3). These data thus suggest that the narrowness of the intercellular space effectively prevents the diffusion of vesicle hydrogels and thereby facilitates their swelling.

The fusion pore of vesicles also acted as a diffusion barrier. To examine the size of fusion pores, we stained exocytic events at the outermost portion of the plasma membrane directly facing the extracellular medium, given that 500-kDa fluorescein dextran did not penetrate the intercellular space (Figure 7B). Exocytic lumens were detected in this region of the plasma membrane, although they were smaller (Figure 3C and G) and markedly less prevalent than those formed in the region of the membrane facing the intercellular space. We found that full-fusion events were stained with 500-kDa fluorescein dextran ( $n=14$ ) (Figure 8A and B), whereas vacuolar events were not ( $n=14$ ) (Figure 8C and D). Given that the vacuolar events were stained with 70-kDa fluorescein dextran (Figure 8E), the diameter of the fusion pore of vacuolar events was estimated to be between 12 and 20 nm.

The fate of vesicles after exocytosis thus depends on the diameter of the fusion pore. If the diameter is  $>20$  nm, vesicles undergo full fusion (16%,  $n=130$ ) (Figure 8A and E); if the diameter is maintained between 12 and 20 nm, the matrix hydrogels are effectively trapped and vesicles undergo vacuolar events (72%) (Figure 8C and E). Swelling of vesicle contents was often followed by full fusion, reflecting subsequent expansion of the pore to a diameter of  $>20$  nm (Figure 7C and D). The 20-nm fusion pore was thus not sufficiently stable in many instances to resist swelling of the vesicle contents. Treatment of the cells with latrunculin A (10  $\mu$ M), an inhibitor of actin polymerization (Coue *et al*, 1987), increased the proportion of full-fusion events to 48% and reduced that of vacuolar events to 38% ( $n=156$ , data not shown), suggesting that cortical F-actin is partly responsible for maintenance of the intermediate fusion pore. SRB staining was retained in the remaining  $\sim 12\%$  of vesicles even after removal of the tracer from the extracellular medium. Most such kiss-and-stay events were not labeled with 70- or 10-kDa fluorescein dextran (Figure 8E and F), indicating that the diameter of the fusion pore was maintained smaller than 6 nm.

### Lateral diffusion of SNAP25 during sequential exocytosis

Our results showed that compound exocytosis was strictly sequential and was not dependent on Ca<sup>2+</sup> gradients in the adrenal medulla, suggesting that secondary exocytosis was

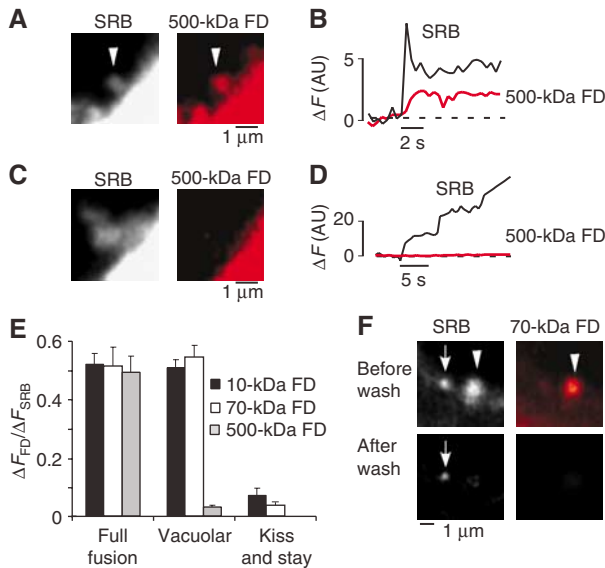


**Figure 8** Role of the fusion pore in determination of vesicle fate after exocytosis. (A, C) A full-fusion event (A) and a vacuolar event (C) at the region of the plasma membrane facing the extracellular medium as revealed by SRB (left) and 500-kDa fluorescein dextran (right). (B, D) Time courses of fluorescence for the vesicles shown in (A) and (C), respectively. (E) Ratio of fluorescence intensities of fluorescein dextran (10, 70, or 500 kDa) and SRB for the same exocytic vesicles. Exocytic events were classified as full fusion, vacuolar, or kiss-and-stay. Fluorescence intensities of fluorescein dextran and SRB for vesicles were normalized by those for the extracellular medium. (F) A kiss-and-stay event (arrow) and a vacuolar event (arrowhead). SRB, but not 70-kDa fluorescein dextran, stained the kiss-and-stay event (before wash), and SRB staining of this event persisted after removal of the dye from the medium (after wash). In contrast, both tracers stained the vacuolar event and staining was lost after dye washout.

triggered by the diffusion of a fusion factor from the primary plasma membrane to the luminal plasma membrane, as has been suggested for other preparations (Nemoto *et al*, 2001; Takahashi *et al*, 2004; Pickett *et al*, 2005). One candidate for such a factor is the SNARE protein SNAP25 (Rothman, 1994). Antibodies to SNAP25 stained the plasma membrane, but not vesicles within the cytoplasm, before stimulation (Figure 9A), whereas they stained vacuolar structures after stimulation (Figure 9B).

Whether SNAP25 is involved in sequential exocytosis had not been tested previously (Guo *et al*, 1998; Nemoto *et al*, 2001; Takahashi *et al*, 2004; Pickett *et al*, 2005). We therefore examined cells transfected with an expression vector for the light chain of botulinum toxin E, an inhibitor of SNAP25 function (Rothman, 1994). We found that the toxin greatly inhibited both primary and secondary exocytosis. The rates of exocytosis were thus  $0.4\text{--}0.7\text{ events min}^{-1}\mu\text{m}^{-2}$  in control cells stimulated with high- $\text{K}^+$  solution (Figure 6A), whereas the rates of primary and secondary exocytosis were reduced to  $0.097 \pm 0.035$  and  $0.038 \pm 0.020\text{ events min}^{-1}\mu\text{m}^{-2}$  (means  $\pm$  s.e.m.,  $n = 38$ ), respectively, in cells transfected with the toxin vector, even though vesicle swelling was similarly detected in both control and transfected cells (data not shown).

We studied the dynamics of the lateral redistribution of SNAP25 by transfecting chromaffin cells with an expression vector for a fusion construct of enhanced cyan fluorescent

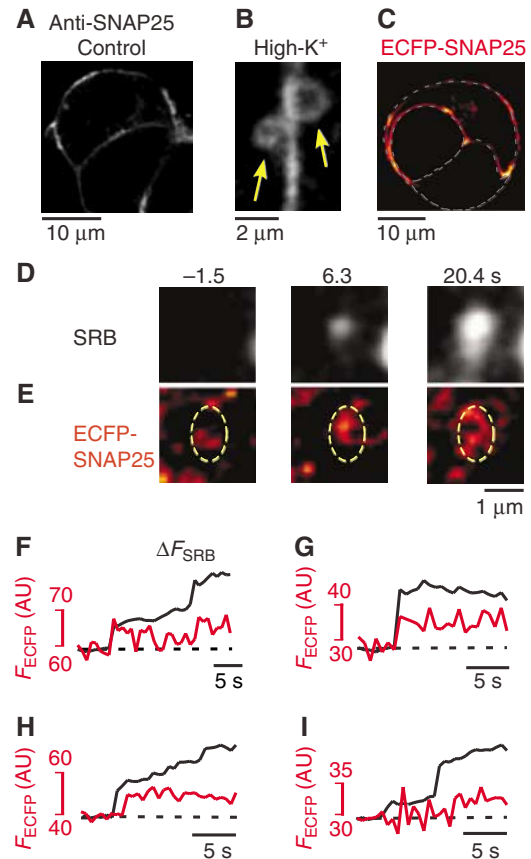


**Figure 9** Distribution of SNAP25 in the adrenal medulla and its lateral diffusion associated with exocytosis. (A, B) Adrenal medullary preparations stained with antibodies to SNAP25 without stimulation (A) and 30 s after high- $\text{K}^+$  stimulation (B). Arrows in (B) indicate vacuolar lumens. (C) Fluorescence of ECFP-SNAP25 in a cluster of transfected adrenal medullary cells without stimulation. Thin dashed lines are outlines of cells that did not express ECFP-SNAP25. (D, E) Simultaneous imaging of SRB (D) and ECFP-SNAP25 (E). Numbers in (D) denote time after the onset of exocytosis. (F–I) Time courses of fluorescence of SRB (black) and ECFP-SNAP25 (red) in four different cells stimulated with high- $\text{K}^+$  solution. The data in (F) were obtained from the outlined region of the cell in (E).

protein (ECFP) and SNAP25. The ECFP-SNAP25 construct selectively stained the plasma membrane before cell stimulation (Figure 9C). Simultaneous multicolor imaging of SRB (Figure 9D) and ECFP-SNAP25 (Figure 9E) revealed that diffusion of ECFP-SNAP25 was apparent soon after vesicle fusion (Figure 9F–I) in 43% of primary exocytic events ( $n = 159$ ). The fluorescence of ECFP-SNAP25 was often at the limit of detection, so that its lateral diffusion might actually occur more frequently. Nevertheless, the value of 43% for detection of SNAP25 redistribution at primary exocytic events in the adrenal medulla is far larger than that (7%) previously determined for pancreatic  $\beta$  cells (Takahashi *et al*, 2004), in which sequential exocytosis constituted only 4% of exocytic events. The mean latency between the onset of exocytosis and the redistribution of ECFP-SNAP25 was  $1.15 \pm 0.16\text{ s}$  ( $n = 45$ ), which is smaller than that (6.3 s) previously determined for  $\beta$  cells (Takahashi *et al*, 2004), where secondary exocytosis occurred slowly with a latency of 17 s. The prevalence and rate of SNAP25 redistribution in the adrenal medulla are thus consistent with the high frequency and speed of sequential exocytosis in this tissue.

## Discussion

With the application of TEP imaging, we have visualized for the first time the formation and fates of the  $\Omega$ -shaped profiles of chromaffin vesicles during exocytosis in the adrenal medulla. The lifetime of the  $\Omega$  profiles was short ( $\sim 0.25$  s), likely explaining why they have been so difficult to detect by electron microscopy (Fox, 1996; Plattner *et al*, 1997). We have found that chromaffin cells frequently manifest a type of sequential exocytosis that extends deep into the cytoplasm, providing us with an opportunity to examine the fusion readiness of vesicles located in this region of the cell. Our characterization of vacuolar sequential exocytosis has also suggested previously unidentified roles for gels within vesicles, the fusion pore, and the extracellular matrix in exocytosis.

### **Two molecular configurations for fusion-ready vesicles**

Our data suggest that the fusion machinery of chromaffin vesicles does not need to be assembled before cell stimulation. Indeed, although the target SNARE protein SNAP25 was found to be necessary for sequential exocytosis, it was absent from the primary vesicles before cell stimulation, being supplied via lateral diffusion from the plasma membrane to the membrane of primary vesicles after their fusion. Furthermore, secondary exocytosis was markedly facilitated by swelling of the exocytic lumen, again indicating that the fusion machinery was not tightly assembled before stimulation. Primary vesicles also underwent exocytosis with similar or smaller rates per membrane area compared with those of deep vesicles. The absence of a preassembled fusion machinery is consistent with the fact that exocytosis is slower for chromaffin vesicles (Ninomiya *et al*, 1997; Haller *et al*, 1998; Voets *et al*, 1999) than for synaptic vesicles in the presynaptic terminal, where preassembly of the fusion machinery is required to account for the submillisecond fusion reaction (Augustine, 2001; Sudhof, 2004; Liu *et al*, 2005).

We therefore propose the two extremes of molecular configurations for fusion-ready vesicles in order to explain  $\text{Ca}^{2+}$ -dependent exocytosis in general. At one extreme, the free configuration, the fusion machinery assembles only after stimulation. Vesicles in the free configuration are localized within a few micrometers from the plasma membrane and may or may not be docked to the plasma membrane before stimulation (prestimulus docking). Such prestimulus docking for vesicles in the free configuration does not serve to hasten the fusion reaction but has other functions (Kishimoto *et al*, 2005). Our present study indicates that most, if not all, chromaffin vesicles located within  $2\ \mu\text{m}$  from the plasma membrane are in the free configuration and possess a similar molecular status in terms of fusion readiness irrespective of their exact distance from the plasma membrane. The free configuration may be a common characteristic of vesicles that mediate regulated exocytosis, given that it appears to be applicable to large dense-core vesicles of chromaffin cells (present study), small vesicles of non-neuronal cells (Liu *et al*, 2005), and yeast vacuoles (Nichols *et al*, 1997; Peters and Mayer, 1998).

At the other extreme, the bound configuration, the fusion machinery assembles and acts before cell stimulation, with the fusion reaction being halted until the final  $\text{Ca}^{2+}$  trigger is provided. The vesicles are bound to the plasma membrane as a result of the prior action of the fusion machinery and

to prevent membrane fusion. The bound configuration is necessary for the fast and synchronous exocytosis of synaptic vesicles; by analogy, it has often been assumed to be required for  $\text{Ca}^{2+}$ -dependent exocytosis in other secretory cells (Martin, 1997; Neher, 1998; Kasai, 1999; Sudhof, 2004). Our present study demonstrates, however, that the bound configuration is not generally applicable to  $\text{Ca}^{2+}$ -dependent exocytosis. Prestimulus docking of only a subpopulation of vesicles is a preparatory step for the bound configuration, and it can persist even after exocytosis (Kishimoto *et al*, 2005), suggesting that prestimulus docking is a parallel reaction that can be independent of the fusion reaction. The bound configuration might represent the hemifusion intermediate of the vesicle and plasma membranes. The precise structural states of the bound configuration, however, have not been directly demonstrated for any biological preparation, including the active zone of presynaptic terminals. It also remains to be determined how fusion is halted in the bound configuration.

The two fusion-ready configurations may coexist in neurons and other secretory cells. The fusion of chromaffin vesicles occurred faster when cells were primed by submicromolar increases in  $[\text{Ca}^{2+}]_i$  for more than 3 min (Haller *et al*, 1998; Voets *et al*, 1999). Similarly, protein kinase A promoted a fast component of exocytosis of insulin vesicles (Takahashi *et al*, 1999; Hatakeyama *et al*, 2006). Such treatments may convert some vesicles in the free configuration to the bound configuration. The two parallel exocytic pathways (Takahashi *et al*, 1997, 1999; Voets *et al*, 1999; Xu *et al*, 1999) might correspond to the two configurations of fusion-ready states described here. Synaptic vesicles also show a slower or asynchronous component of release (Goda and Stevens, 1994; Nishiki and Augustine, 2004; Sudhof, 2004), which might reflect the free configuration of small vesicles (Liu *et al*, 2005). Intermediates of two extreme configurations might exist, and account for the large variability in the rates of exocytosis in different preparations (Kasai, 1999).

### **Vacuolar sequential exocytosis**

We have found that swelling of gels within fused vesicles facilitates subsequent fusion reactions for deep vesicles. Swelling of vesicles after fusion has been described previously for adrenal chromaffin cells and mast cells (Zimmerberg *et al*, 1987; Amatore *et al*, 2000), and it has been implicated in postfusion control of the fusion pore (Rahamimoff and Fernandez, 1997). Our study extends these previous observations and suggests that swelling of exocytic vesicles exerts prefusion control of exocytosis. Sequential exocytosis was preferentially induced at regions of the plasma membrane facing the intercellular space, where diffusion of the intravesicular gels was prevented. The extracellular matrix of the intercellular space thus facilitates swelling of the intravesicular gels and plays an important role in the mobilization of deep vesicles in intact tissue.

Maintenance of a narrow fusion pore also facilitates sequential exocytosis by promoting the expansion of round lumens deep into the cytoplasm. The stabilization of such pores appears to require the membrane cytoskeleton, given that removal of cortical F-actin by treatment of cells with latrunculin A reduced the frequency of vacuolar events by half. Prestimulus docking of vesicles in chromaffin cells (Steyer *et al*, 1997) may also contribute to stabilization of

the fusion pore (Kishimoto *et al*, 2005). Indeed, quick-freeze deep-etch electron microscopic analysis of chromaffin cells revealed fine strands connecting vesicles to the plasma membrane that persisted after the fusion reaction and which may comprise annexins (Nakata *et al*, 1990).

In typical sequential exocytosis in pancreatic acini, beaded strands of vesicles are preserved (Ichikawa, 1965; Nemoto *et al*, 2001) by rapid coating of fused vesicles with F-actin (Nemoto *et al*, 2004). Prevention of such actin polymerization results in vacuole formation similar to that observed in chromaffin cells (Nemoto *et al*, 2004) and leads to destruction of polarity of the acinus and intravacuolar activation of vesicle enzymes, both of which may contribute to the pathogenesis of acute pancreatitis (Raraty *et al*, 2000). Secretory polarity is almost absent in chromaffin cells compared with acinar cells, and no digestive enzymes are present within chromaffin vesicles. Thus, coating of vesicles with F-actin is not induced by stimulation in chromaffin cells (Vitale *et al*, 1995), and swelling of the exocytic lumen functions to mobilize vesicles in the deep cytoplasmic layers of these cells, especially during intensive stimulation.

In summary, we have revealed that chromaffin vesicles located within 2  $\mu\text{m}$  from the plasma membrane may be fusion ready in the free configuration, given that exocytosis readily proceeded to the fourth layer of vesicles. Such fusion-ready vesicles constitute at most 64% ( $100\% (7^3 - 5^3) / 7^3$ ) of all vesicles, assuming the radius of a chromaffin cell is 7  $\mu\text{m}$ . Vacuolar sequential exocytosis in the intact adrenal gland allows the efficient mobilization on demand of vesicles in the deeper layers of the cytoplasm and is dependent on the large pool of fusion-ready vesicles present deep within the cytoplasm, the postfusion swelling of gels present within the vesicles, a narrow fusion pore, and the extracellular matrix.

## Materials and methods

### Preparations

Most experiments were performed with porcine adrenal medulla, although bovine adrenal medulla was used for some initial experiments. There were no systematic differences in results obtained between the two species, and the data presented are from pig unless indicated otherwise. The adrenal medulla was briefly treated with collagenase and subjected to gentle trituration to obtain small clusters of cells. The clusters were maintained on collagen-coated glass coverslips for 1–5 days in Dulbecco's modified Eagle's medium supplemented with 7% fetal bovine serum and 7% horse serum, as described previously (Ninomiya *et al*, 1997). For experiments, the cell clusters were immersed in a solution containing 140 mM NaCl, 5 mM KCl, 2 mM  $\text{CaCl}_2$ , 1 mM  $\text{MgCl}_2$ , 10 mM Hepes–NaOH (pH 7.3), and 10 mM glucose. The cells were loaded with NPE by incubation for 30 min with 30  $\mu\text{M}$  of the corresponding acetoxymethyl ester (Molecular Probes, Eugene, OR) in serum-free culture medium; in some experiments, they were also incubated with 10  $\mu\text{M}$  of the acetoxymethyl ester of fura-2FF (TEF Labs, Austin, TX). The polar fluorescent tracer SRB (0.5–0.7 mM) (Molecular Probes) was added to the cell clusters 10 min before stimulation. In some experiments, Ficoll (Amersham Biosciences, Piscataway, NJ) was also added. Uncaging of NPE was induced with a mercury lamp (U-ULS100HG; Olympus, Tokyo, Japan) through a 360-nm band-pass filter. The radiation of the mercury lamp was gated with an electric shutter (IX-ESU, Olympus) with an opening duration of 250 ms. Fluorescein dextran (10, 70, or 500 kDa) (Molecular Probes) was applied locally at 2 mM to the cell clusters with a glass pipette. The diameters of the dextran molecules were estimated as 6, 12, and 20 nm for 10-, 70-, and 500-kDa dextran, respectively, on the basis of the previously published value of 6 nm for 10-kDa dextran (Ioan *et al*, 2000).

### TEP imaging

TEP imaging was performed with an inverted microscope (IX70, Olympus) and a laser-scanning microscope (FV300, Olympus) and with a water immersion objective lens (UPlanApo  $\times 60$  water/IR; numerical aperture, 1.2) as described (Nemoto *et al*, 2001; Takahashi *et al*, 2002; Kasai *et al*, 2005). The laser power at the specimen was 3–10 mW and the wavelength was 830 nm. Polar tracers and ECFP were excited at 830 nm. Simultaneous measurement of SRB and either fluorescein dextran or ECFP fluorescence was performed with a dichroic mirror (corner wavelength of 570 nm) and two photomultipliers. Fluorescence intensities of SRB, fluorescein dextran, and ECFP were measured at 570–650, 420–530, and 400–510 nm, respectively. Images were acquired every 0.1–2 s at a plane 5–30  $\mu\text{m}$  from the glass coverslip. FWHM diameters of 0.1- $\mu\text{m}$ -diameter fluorescent beads were 0.32  $\mu\text{m}$  laterally and 1.4  $\mu\text{m}$  axially. TEPIQ analyses of  $\Delta V$  or  $\Delta S$  were performed by using  $p_{xy}(0) = 0.56$  as described (Kasai *et al*, 2005) and using  $m_c = 0.305 \pm 0.063$  (mean  $\pm$  s.d.,  $n = 9$ ) obtained for chromaffin cells. Twelve-bit images were color coded with either the fall or gray codes of FV300. Imaging experiments were performed at room temperature (24–25°C).

We counted the number of exocytic events whose fluorescence intensity was  $>20\%$  of the maximal value; these events would be expected to occur within 1  $\mu\text{m}$  from the focal plane, given the axial resolution of 1.4  $\mu\text{m}$  of our setup (Kasai *et al*, 2005). In other words, the thickness of our image for detection of exocytosis was 2  $\mu\text{m}$  ( $= T$ ) along the  $z$ -axis. To estimate the membrane area and volume of an exocytic lumen (Figures 4–6), we assumed (for simplicity) the lumen to be a cylinder (rather than a sphere) along the  $z$ -axis with a radius of  $R_i(t)$ . Provided that exocytosis occurs homogeneously around the lumen, the exocytic events that we counted should give rise to the swelling of a section of the lumen with a  $z$ -axis length of 2  $\mu\text{m}$  ( $= T$ ). The corresponding membrane area and volume of the lumen were therefore estimated as  $2\pi R_i(t)T$  and  $\pi R_i(t)^2 T$ , respectively. The value of  $T$  affects our estimate of the swelling ratio but not the comparison of fusion readiness between primary and secondary vesicles.

### Immunohistochemistry

Cell clusters were fixed after experiments with 4% paraformaldehyde and then permeabilized with 0.1% Triton X-100 in phosphate-buffered saline containing 0.6% bovine serum albumin. They were then incubated for 45 min at room temperature with a mouse monoclonal antibody to SNAP25 (Wako, Osaka, Japan) diluted 1:100 with phosphate-buffered saline containing 0.6% bovine serum albumin. Immune complexes were detected with Bodipy FL-coupled goat antibodies to mouse immunoglobulin G (1:200 dilution) (Molecular Probes).

### Transfection

The DNA sequence encoding the light chain of botulinum toxin E (kindly provided by H Gaisano) was inserted into the multicloning site of the expression vector pECFP-C1 (Clontech, Mountain View, CA). Adrenal medullary tissue was incubated with the resulting vector, pECFP-C1-BTX-E (6  $\mu\text{g ml}^{-1}$ ), for 3–4 h in serum-free medium containing Lipofectamine 2000 (Gibco), washed, and then incubated for an additional 12–24 h before experiments. Alternatively, cell clusters were infected with an adenoviral vector ( $7 \times 10^7$  plaque-forming units  $\text{ml}^{-1}$ ) encoding an ECFP fusion construct of SNAP25 for 2 h in serum-free culture medium as described (Takahashi *et al*, 2004); they were then washed and incubated for an additional 10–18 h before experiments.

### Supplementary data

Supplementary data are available at *The EMBO Journal* Online.

## Acknowledgements

We thank R Ijuin and N Takahashi for technical assistance, H Gaisano for the plasmid encoding the light chain of botulinum toxin E, H Okado and A Miwa for the adenoviral vector, and P Somogyi for helpful discussion. This work was supported by Grants-in-Aid from the Japanese Ministry of Education, Culture, Sports, Science, and Technology and from the Japanese Society for the Promotion of Science, as well as by research grants from the Human Frontier Science Program Organization and Takeda Science Foundation.

## References

- Alvarez de Toledo G, Fernandez JM (1990) Compound versus multigranular exocytosis in peritoneal mast cells. *J Gen Physiol* **95**: 397–409
- Amatore C, Bouret Y, Travis ER, Wightman RM (2000) Interplay between membrane dynamics, diffusion and swelling pressure governs individual vesicular exocytotic events during release of adrenaline by chromaffin cells. *Biochimie* **82**: 481–496
- Angleson JK, Cochilla AJ, Kilic G, Nussinovitch I, Betz WJ (1999) Regulation of dense core release from neuroendocrine cells revealed by imaging single exocytotic events. *Nat Neurosci* **2**: 440–446
- Augustine GJ (2001) How does calcium trigger neurotransmitter release? *Curr Opin Neurobiol* **11**: 320–326
- Baker PF, Knight DE (1981) Calcium control of exocytosis and endocytosis in bovine adrenal medullary cells. *Philos Trans R Soc London B* **296**: 83–103
- Benedeczy I, Somogyi P (1975) Ultrastructure of the adrenal medulla of normal and insulin-treated hamsters. *Cell Tissue Res* **162**: 541–550
- Chow RH, Klingauf J, Heinemann C, Zucker RS, Neher E (1996) Mechanisms determining the time course of secretion in neuroendocrine cells. *Neuron* **16**: 359–376
- Coue M, Brenner SL, Spector I, Korn ED (1987) Inhibition of actin polymerization by latrunculin A. *FEBS Lett* **213**: 316–318
- Fox GQ (1996) A morphometric analysis of exocytosis in KCl-stimulated bovine chromaffin cells. *Cell Tissue Res* **284**: 303–316
- Furuya S, Edwards C, Ornberg RL (1989) Exocytosis of bovine chromaffin granules in Ficoll captured by rapid freezing. *J Electron Microscop* **38**: 143–147
- Goda Y, Stevens CF (1994) Two components of transmitter release at a central synapse. *Proc Natl Acad Sci USA* **91**: 12942–12946
- Guo Z, Turner C, Castle D (1998) Relocation of the t-SNARE SNAP-23 from lamellipodia-like cell surface projections regulates compound exocytosis in mast cells. *Cell* **94**: 537–548
- Haller M, Heinemann C, Chow RH, Heidelberger R, Neher E (1998) Comparison of secretory responses as measured by membrane capacitance and by amperometry. *Biophys J* **74**: 2100–2113
- Hatakeyama H, Kishimoto T, Nemoto T, Kasai H, Takahashi N (2006) Rapid glucose sensing by protein kinase A for insulin exocytosis in mouse pancreatic islets. *J Physiol* **570**: 271–282
- Ichikawa A (1965) Fine structural changes in response to hormonal stimulation of the perfused canine pancreas. *J Cell Biol* **24**: 369–385
- Ioan C, Aberle T, Burchard W (2000) Structural properties of dextran. 2. Dilute solution. *Macromolecules* **33**: 5730–5739
- Kasai H (1999) Comparative biology of exocytosis: implications of kinetic diversity for secretory function. *Trends Neurosci* **22**: 88–93
- Kasai H, Hatakeyama H, Kishimoto T, Liu TT, Nemoto T, Takahashi N (2005) A new quantitative (TEPIQ) analysis for diameters of exocytotic vesicles and its application to mouse pancreatic islets. *J Physiol* **568**: 891–903
- Kishimoto T, Liu TT, Hatakeyama H, Nemoto T, Takahashi N, Kasai H (2005) Sequential compound exocytosis of large dense-core vesicles in PC12 cells studied with TEPIQ analysis. *J Physiol* **568**: 905–915
- Liu TT, Kishimoto T, Hatakeyama H, Nemoto T, Takahashi N, Kasai H (2005) Exocytosis and endocytosis of small vesicles in PC12 cells studied with TEPIQ analysis. *J Physiol* **568**: 917–929
- Martin TFJ (1997) Stages of regulated exocytosis. *Trends Cell Biol* **7**: 271–276
- Nakata T, Sobue K, Hirokawa N (1990) Conformational change and localization of calpactin I complex involved in exocytosis as revealed by quick-freeze, deep-etch electron microscopy and immunocytochemistry. *J Cell Biol* **110**: 13–25
- Nanavati C, Fernandez JM (1993) The secretory granule matrix: a fast-acting smart polymer. *Science* **259**: 963–965
- Neher E (1998) Vesicle pools and Ca<sup>2+</sup> microdomains: new tools for understanding their roles in neurotransmitter release. *Neuron* **20**: 389–399
- Nemoto T, Kimura R, Ito K, Tachikawa A, Miyashita Y, Iino M, Kasai H (2001) Sequential-replenishment mechanism of exocytosis in pancreatic acini. *Nat Cell Biol* **3**: 253–258
- Nemoto T, Kojima T, Oshima A, Bito H, Kasai H (2004) Stabilization of exocytosis by dynamic F-actin coating of zymogen granules in pancreatic acini. *J Biol Chem* **279**: 37544–37550
- Nichols BJ, Ungermann C, Pelham HRB, Wickner WT, Haas A (1997) Homotypic vacuolar fusion mediated by t- and v-SNAREs. *Nature* **387**: 199–202
- Ninomiya Y, Kishimoto T, Yamazawa T, Ikeda H, Miyashita Y, Kasai H (1997) Kinetic diversity in the fusion of exocytotic vesicles. *EMBO J* **16**: 929–934
- Nishiki T, Augustine GJ (2004) Synaptotagmin I synchronizes transmitter release in mouse hippocampal neurons. *J Neurosci* **24**: 6127–6132
- Peters C, Mayer A (1998) Ca<sup>2+</sup>/calmodulin signals the completion of docking and triggers a late step of vacuole fusion. *Nature* **396**: 575–580
- Pickett JA, Thorn P, Edwardson JM (2005) The plasma membrane Q-SNARE syntaxin 2 enters the zymogen granule membrane during exocytosis in the pancreatic acinar cell. *J Biol Chem* **280**: 1506–1511
- Plattner H, Artalejo AR, Neher E (1997) Ultrastructural organization of bovine chromaffin cell cortex-analysis by cryofixation and morphometry of aspects pertinent to exocytosis. *J Cell Biol* **139**: 1709–1717
- Rahamimoff R, Fernandez JM (1997) Pre- and postfusion regulation of transmitter release. *Neuron* **18**: 17–27
- Raraty M, Ward J, Erdemli G, Vaillant C, Neoptolemos JP, Sutton R, Petersen OH (2000) Calcium-dependent enzyme activation and vacuole formation in the apical granular region of pancreatic acinar cells. *Proc Natl Acad Sci USA* **97**: 13126–13131
- Rothman JE (1994) Mechanisms of intracellular protein transport. *Nature* **372**: 55–63
- Steyer JA, Horstmann H, Almers W (1997) Transport, docking and exocytosis of single secretory granules in live chromaffin cells. *Nature* **388**: 474–478
- Sudhof TC (2004) The synaptic vesicle cycle. *Annu Rev Neurosci* **27**: 509–547
- Takahashi N, Hatakeyama H, Okado H, Miwa A, Kishimoto T, Kojima T, Abe T, Kasai H (2004) Sequential exocytosis of insulin granules is associated with redistribution of SNAP25. *J Cell Biol* **165**: 255–262
- Takahashi N, Kadowaki T, Yazaki Y, Elis-Davies GCR, Miyashita Y, Kasai H (1999) Post-priming actions of ATP in the Ca<sup>2+</sup> dependent exocytosis in pancreatic  $\beta$ -cells. *Proc Natl Acad Sci USA* **96**: 760–765
- Takahashi N, Kadowaki T, Yazaki Y, Miyashita Y, Kasai H (1997) Multiple exocytotic pathways in pancreatic  $\beta$  cells. *J Cell Biol* **138**: 55–64
- Takahashi N, Kishimoto T, Nemoto T, Kadowaki T, Kasai H (2002) Fusion pore dynamics and insulin granule exocytosis in the pancreatic islet. *Science* **297**: 1349–1352
- Tanaka T, Nishio I, Sun ST, Uenonishio S (1982) Collapse of gels in an electric-field. *Science* **218**: 467–469
- Vitale ML, Seward EP, Trifaro JM (1995) Chromaffin cell cortical actin network dynamics control the size of the release-ready vesicle pool and the initial rate of exocytosis. *Neuron* **14**: 353–363
- Voets T, Neher E, Moser T (1999) Mechanisms underlying phasic and sustained secretion in chromaffin cells from mouse adrenal slices. *Neuron* **23**: 607–615
- Xu T, Rammner B, Margittai M, Artalejo AR, Neher E, Jahn R (1999) Inhibition of SNARE complex assembly differentially affects kinetic components of exocytosis. *Cell* **99**: 713–722
- Zimmerberg J, Curran M, Cohen FS, Brodwick M (1987) Simultaneous electrical and optical measurements show that membrane fusion precedes secretory granule swelling during exocytosis of beige mouse mast cells. *Proc Natl Acad Sci USA* **84**: 1585–1589